PCCP

Accepted Manuscript

This article can be cited before page numbers have been issued, to do this please use: P. A. Panchenko, M. A. Grin, O. Fedorova, M. A. Zakharko, D. A. Pritmov , A. F. Mironov, A. N. Arkhipova, Y. V. Fedorov, G. Jonusauskas, R. I. Yakubovskaya, N. B. Morozova, A. A. Ignatova and A. Feofanov, *Phys. Chem. Chem. Phys.*, 2017, DOI: 10.1039/C7CP04449F.

ROYAL SOCIETY OF CHEMISTRY

rsc.li/pccp

View Article Online
DOI: 10.1039/C7CP04449F

View Article Online
DOI: 10.1039/C7CP04449F

Novel Bacteriochlorin–Styrylnaphthalimide Conjugate for Simultaneous Photodynamic Therapy and Fluorescence Imaging

Pavel A. Panchenko,[a,b,*] Mikhail A. Grin,[c] Olga A. Fedorova,[a,b] Marina A. Zakharko,[a] Dmitriy A. Pritmov,[c] Andrey F. Mironov,[c] Antonina N. Arkhipova,[a] Yuri V. Fedorov,[a] Gediminas Jonusauskas,[d] Raisa I. Yakubovskaya,[e] Natalia B. Morozova,[e] Anastasia A. Ignatova[f,g] and Alexey V. Feofanov[f,g]

[a]*A. N. Nesmeyanov Institute of Organoelement Compounds of Russian Academy of Sciences, 119991, Vavilova str. 28, Moscow, Russia,*
Tel.: +7 499 135 80 98, Fax: +7 499 135 50 85, E-mail: pavel@ineos.ac.ru
[b]*D. Mendeleev University of Chemical Technology of Russia, 125047, Miusskaya sqr. 9, Moscow, Russia,*
[c]*Moscow Technological University, Institute of Fine Chemical Technologies, 119571, Prospect Vernadskogo, 86, Moscow, Russia,*
[d]*Laboratoire Ondes et Matière d'Aquitaine, UMR CNRS 5798, Bordeaux University, 33405, 351 Cours de la Libération, Talence, France,*
[e]*P. Hertsen Moscow Oncology Research Institute – Branch of the National Medical Research Radiological Centre of the Ministry of Health of the Russian Federation, 125284, 2nd Botkinskiy pr. 3, Moscow, Russia,*
[f]*Biological Faculty, Lomonosov Moscow State University, 119992, Leninskie Gory 1, Moscow, Russia.*
[g]*Shemyakin-Ovchinnikov Institute of Bioorganic Chemistry of Russian Academy of Sciences, 117997, Miklukho-Maklaya str., 16/10, Moscow, Russia*

Abstract

Propargyl-15^2,17^3-dimethoxy-13^1-amide of bacteriochlorin *e* (**BChl**) and 4-(4-*N*,*N*-dimethylaminostyryl)-*N*-alkyl-1,8-naphthalimide bearing azide group in the *N*-alkyl fragment were conjugated by the copper(I)-catalyzed 1,3-dipolar cycloaddition to produce novel dyad compound **BChl-NI** for anticancer photodynamic therapy (PDT) combing the modalities of a photosensitizer (PS) and a fluorescent imaging agent. A precise photophysical investigation of the conjugate in solution using steady-state and time-resolved optical spectroscopies revealed that the presence of naphthalimide (NI) fragment does not decrease the photosensitizing ability of the bacteriochlorin (BChl) core as compared with **BChl**, however, the fluorescence of naphthalimide is completely quenched due to resonance energy transfer (RET) to BChl. It has

View Article Online
DOI: 10.1039/C7CP04449F

been shown that conjugate **BChl-NI** penetrates into human lung adenocarcinoma A549 cells, accumulates in the cytoplasm where it has a mixed granular-diffuse distribution. Both NI and BChl fluorescence *in vitro* provides registration of bright images showing perfectly intracellular distribution of **BChl-NI**. The ability of NI to emit light upon excitation in imaging experiments has been found to be due to hampering of RET as a result of photodestruction of energy acceptor BChl unit. Phototoxicity studies have shown that conjugate **BChl-NI** is not toxic for A549 cells at tested concentrations (<8 μM) without light-induced activation. At the same time, the concentration-dependent killing of cells is observed upon the excitation of bacteriochlorin moiety with the red light that occurs due to reactive oxygen species formation. The presented data demonstarte that conjugate **BChl-NI** is a promissing dual function agent for cancer diagnostics and therapy.

Keywords

Photodynamic therapy, naphthalimide, bacteriochlorin, click chemistry, fluorescent imaging, photosensitizer, resonance energy transfer

Graphical Abstract

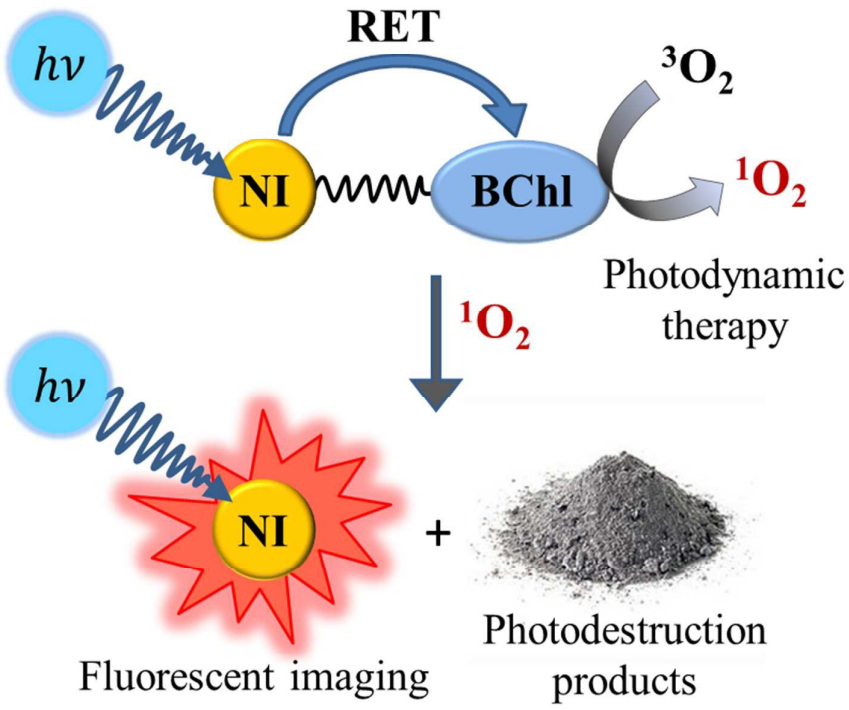

Textual abstract for the table of contents entry

Photosensitizing and fluorescence imaging ability of bacteriochlorin–naphthalimide conjugate is studied

View Article Online
DOI: 10.1039/C7CP04449F

1. Introduction

Photodynamic therapy (PDT) has emerged as an important treatment modality for a variety of cancers in recent years.[1,2] PDT involves three necessary components: light, photosensitizer (PS), and tissue molecular oxygen. Upon irradiation by light of appropriate wavelength, PS is promoted to a short lived singlet state which rapidly converts to excited triplet state (^{3}PS*) through the process of intersystem crossing. Then, ^{3}PS* transfers its excess energy to nearby O_2 molecules to form reactive oxygen species such as singlet oxygen ($^1O_2$) and free radicals, which are toxic to malignant cells and tissues.[3–6]

Among various photosensitizing agents, porphyrin-based compounds possess unique advantages related to their ability to be retained in tumors and to produce cytotoxic singlet oxygen. Photofrin, porphyrin-type PS of the first generation, has achieved some clinical efficacy, but at the same time it suffered from several drawbacks such as chemical heterogeneity, low depth of tissue treatment caused by limited light penetration due to absorption wavelength (630 nm) laying outside "phototherapeutic window" (650 – 1350 nm), low molar extinction coefficient at 630 nm, and prolonged cutaneous photosensitivity caused by its slow elimination in normal tissue.[7] Compared to porphyrins, chlorin- and bacteriochlorin-type PSs in which one or two pyrrole units (diagonal to each other) are reduced respectively exhibit intense absorption in the near infrared region ($\geq$ 650 nm), relatively low dark toxicities, rapid clearance from normal tissue and low cutaneous phototoxicity.[8–13] Despite smaller synthetic availability, di- and tetrahydroporphyrins could be considered as one of the most promising candidates for creating efficient second-generation drugs for PDT of cancer.

An important characteristic of most of the porphyrin-based photosensitizers is their ability to fluoresce. This property has been extensively explored in pre-clinical and clinical studies for fluorescence-image guided PDT. Unfortunately, porphyrins, chlorins, and bacteriochlorins display small Stokes shift between their longer wavelength absorption and emission bands[14–16] and, therefore, their fluorescence is difficult to filter out of the scattered excitation light. This property of the PS fluorescence complicates imaging of deeply seated and large tumors. On the other hand, excitation of the porphyrin-based photosensitizer ultimately leads to the production of reactive oxygen species and related toxicity.[14–17]

To overcome this difficulty a new approach which consists in the construction of bifunctional systems combining modalities of PS and diagnostic agent (so called theranostics) has been developed.[18–22] In such systems, fluorescent moiety can be excited selectively and independently from the photosensitizer unit enabling fluorescence imaging without toxic effects. Thus, Pandey and coworkers have used cyanine dyes as fluorescent labels to prepare conjugates with PSs.[18–20] A distinct feature of the emission spectra of cyanine dyes is that their fluorescence

View Article Online
DOI: 10.1039/C7CP04449F

can easily reach near-infrared (NIR) region upon increasing the length of polymethine chain.[23] However, polymethine cyanine dyes are not so easy to synthesize and to modify, their photostabilities are relatively low and their Stokes shift is usually less than 25 nm, which may cause self-quenching as well as the increase of measurement error due to detection of scattered excitation, thus decreasing the detection sensitivity to a great extent as it is in the case of using simple porphyrin sensitizers. Some examples of BODIPY–phthalocyanine[24,25] and rhodamine–phthalocyanine[26,27] conjugates have also been described in literature. Despite the higher photostability of BODIPY and rhodamine derivatives as compared with cyanine dyes, these types of fluorophores also demonstrate small difference between absorption and emission maxima. Therefore, NIR dyes with a larger Stokes shift are very promising for the development of bifunctional conjugates for simultaneous photodynamic therapy and fluorescent imaging.

1,8-Naphthalimide derivatives are famous organic fluorophores which generally exhibit high thermo and photostability and are known to act as fluorescent brighteners and dyes for polymer fibers,[28,29] laser active media,[30,31] electroluminescent materials[32–34] and optical memory devices.[35–37] Because of its intense fluorescence, large Stokes shifts along with the relative ease of synthetic operations for targeted modification of the molecular structure, this type of compounds has found application in the construction of fluorescent chemosensors for biologically relevant cations and anions,[38–40] labels or probes for proteins, cells, lysosomes and other acidic organelles.[41–43] In our recent papers,[44–46] we have described photophysical properties of naphthalimides containing substituted styryl fragment as an electron releasing group at the 4th position of naphthalene ring. It has been found that the presence of 4-(*N*,*N*-dimethylamino)styryl group extends the π-system of the parent chromophore and results in the long wavelength intramolecular charge transfer (ICT) absorption and emission, which is preferable for fluorescence imaging. Herein, we report on the synthesis, spectroscopic investigation and evaluation of PDT activity of novel conjugate of bacteriochlorin photosensitizer and 4-(*N*,*N*-dimethylamino)styryl-1,8-naphthalimide (**BChl-NI**, Scheme 1). The results and experimental details of our study of optical properties of this molecular system in solution and in living cells are presented. We report on distinct photo-induced cytotoxicity of **BChl-NI** for human adenocarcinoma A549 cells as well as red-to-green conversion of **BChl-NI** fluorescence that can be useful to control integrity of photosensitizer moiety during irradiation of cancer cells.

View Article Online
DOI: 10.1039/C7CP04449F

2. Experimental procedures

Synthesis of conjugate BChl-NI. For the synthesis of **BChl-NI**, we used the well-known copper(I)-catalyzed click reaction of 1,3-dipolar cycloaddition between naphthalimide-containing alkylazide **NI6** and triple bond derivative of bacteriochlorin *e* **BChl** (Scheme 1). The latter was afforded from methyl ester of bacteriopheophorbide *a* **BPheid** and propargylamine. Preparation of **BPheid** starting from biomass *Rhodobacter capsulatus* was carried out according to described method.[47,48] The first step of the synthesis of naphthalimide **NI6**, in which commercial starting material 4-bromo-1,8-naphthalic anhydride was reacted with ethanolamine, was performed conveniently in EtOH at reflux.[49] Next, 4-bromnaphthalimide **NI1** was subjected to the Heck coupling reaction with 4-*N*,*N*-dimethylaminostyrene under catalyst $Pd(OAc)_2$[50] followed by the nucleophilic substitution of hydroxyl by azide group in the hydroxyethyl fragment *via* subsequent treatment with $POCl_3$ and NaN_3. Details of synthetic procedures and identifications are shown in the Supplementary Information. Synthesis of *N*-butyl-4-styrylnaphthalimide **NI4** which was used for comparative analysis of spectral characteristics has been described earlier.[44]

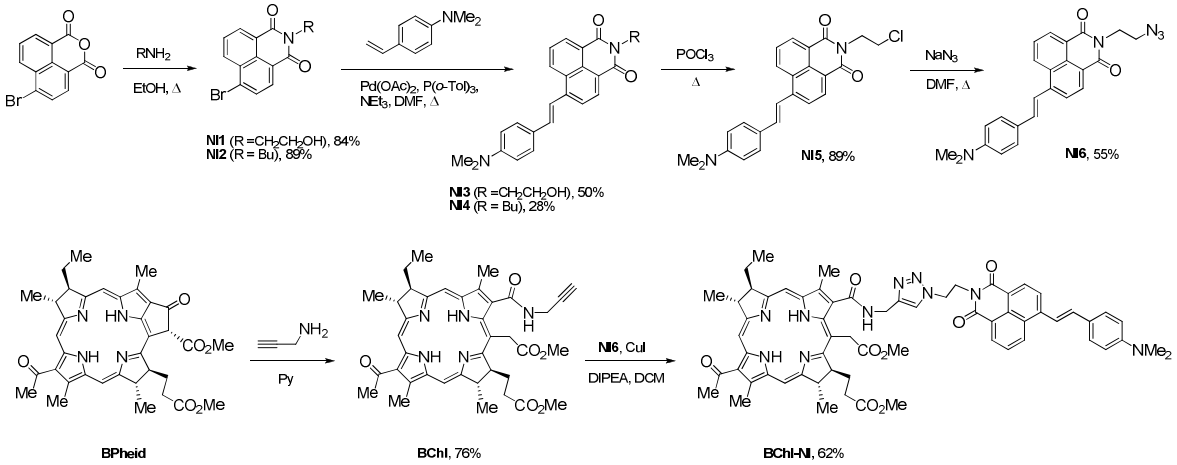

Scheme 1. Synthesis of **BChl**, **NI1–6** and **BChl–NI**

Steady-state optical measurements. The absorption spectra were taken on a Varian-Cary 5G spectrophotometer. The fluorescence quantum yield measurements were performed using a Varian-Cary 5G spectrophotometer and a FluoroLog-3 spectrofluorimeter. Spectral measurements were carried out in air-saturated acetonitrile solutions (acetonitrile of spectrophotometric grade, water content <0.005%, Aldrich) at 20 ± 1 ºC; the concentrations of studied compounds were of about $0.5–2.0 \cdot 10^{-5}$ M. All measured fluorescence spectra were corrected for the nonuniformity of detector spectral sensitivity. Coumarin 481 in acetonitrile (φ^{fl} = 0.08)[51] was used as a reference for the fluorescence quantum yield measurements. The fluorescence quantum yields were calculated by the Eq.(1),[52]

View Article Online
DOI: 10.1039/C7CP04449F

$$\varphi^{\mathrm{fl}} = \varphi_{\mathrm{R}}^{\mathrm{fl}} \frac{S}{S_{\mathrm{R}}} \cdot \frac{(1-10^{-A_{\mathrm{R}}})n^2}{(1-10^{-A})n_{\mathrm{R}}^2} \quad (1)$$

wherein φ^{fl} and $\varphi_{\mathrm{R}}^{\mathrm{fl}}$ are the fluorescence quantum yields of the studied solution and the standard compound respectively; A and A_{R} are the absorptions of the studied solution and the standard respectively; S and S_{R} are the areas underneath the curves of the fluorescence spectra of the studied solution and the standard respectively; and n and n_{R} are the refraction indices of the solvents for the substance under study and the standard compound.

Quantum yields of singlet oxygen generation. The quantum yields of singlet oxygen (Φ_Δ) were estimated in acetone by using tetraphenylporphirin (TPP) as a reference compound ($\Phi_\Delta^{\mathrm{TPP}}$= 0.7)[53,54] and 1,3-diphenylisobenzofuran (DPBF) as a $^1O_2$ trap. In a typical experiment, solutions (2.5 ml) containing both PSs (TPP and PS under study) and DPBF were placed into 1 cm rectangular spectroscopic cells and irradiated by monochromatic light (510 nm) using the excitation unit (a xenon lamp and excitation monochromator) of the FluoroLog-3 fluorimeter. The initial concentration of DPBF corresponded to absorption of about 1 at 414 nm (~40 mM). Identical initial DPBF concentrations were used for the reference solution of TPP and the samples. The change in DPBF absorption at 414 nm was recorded as a function of irradiation time *via* UV/Vis spectrometry. The values of Φ_Δ were calculated by the Eq.(2),

$$\Phi_\Delta = \Phi_\Delta^{\mathrm{R}} \frac{V}{V_{\mathrm{R}}} \cdot \frac{1-10^{-A_{\mathrm{R}}}}{1-10^{-A}} \quad (2)$$

wherein V and V_{R} are the bleaching rates of the solutions containing PS under study (V) and reference compound (V_{R}) which were found from the slopes of linear plots of absorption at 414 nm *versus* irradiation time; A and A_{R} are absorption values at excitation wavelength (510 nm) of the solutions containing studied PS and reference compound (TPP) respectively. The accuracy of Φ_Δ estimation was about 10%.

Subpicosecond transient absorption setup. A Ti:sapphire laser system output (0.6 mJ and 30 fs at 800 nm and 1 kHz pulse repetition rate (Femtopower Compact Pro)) was split in two parts, producing the pump and the probe beams. 80% of pulses were used to pump an optical parametric generator (TOPAS (Light Conversion)) to generate the wavelength tuneable pump pulse. Following TOPAS, the harmonic generation or frequency mixing in a nonlinear crystal produced the excitation pulses in the range 250 – 2600 nm. The probe was a white light continuum pulse, extending from 390 nm to 900 nm, generated by focusing the 800 nm pulses (~5 μJ per pulse) into a 5 mm thick D_2O cell. The variable delay time between excitation and probe pulses was obtained by using a delay line with 0.1 mm resolution. The solutions were placed in a 1 mm circulating cell. Whitelight signal and reference spectra were recorded with a two-channel fiber spectrometer (Avantes Avaspec-2048-2). A home-written acquisition and

View Article Online
DOI: 10.1039/C7CP04449F

experiment-control program in LabView made it possible to record transient spectra with an average error of less than 10^{-3} of O.D. The temporal resolution of our setup was better than 60 fs. Temporal chirp of the probe pulse was corrected by a computer program with respect to a Lawrencian fit of a Kerr signal generated in a 0.2 mm glass plate used in a place of the sample.

Nanosecond transient absorption setup. A frequency tripled Nd:YAG amplified laser system (30 ps, 30 mJ @1064nm, 20 Hz, Ekspla model PL 2143) output was used to pump an optical parametric generator (Ekspla model PG 401) producing tunable excitation pulses in the range 410 – 2300 nm. The residual fundamental laser radiation was focused in a high pressure Xe filled breakdown cell where a white light pulse for sample probing was produced. All signals were analyzed by a spectrograph (Princeton Instruments Acton model SP2300) coupled with a high dynamic range streak camera (Hamamatsu C7700, 1ns-1ms). Accumulated sequences (sample emission, probe without and with excitation) of pulses were recorded and treated by HPDTA (Hamamatsu) software to produce two-dimentional maps (wavelength *versus* delay) of transient absorption intensity in the range 300 – 800 nm. Typical measurement error was better than 10^{-3} O.D.

Fluorescent imaging and procedure of photodynamic treatment of tumor cells. Human lung adenocarcinoma A549 cells were grown (37 °C, 5% CO_2) in Eagle's minimum essential medium with phenol red, 8% fetal calf serum, 2 mM L-glutamine (so called complete medium). The cells were subcultured twice per week. On the day prior to an experiment, an exponentially growing cells were plated on a round cover glasses placed in 24-well plates (for microscopic experiments) or seeded directly in 96-well plates (for cytotoxicity measurements). Sowing density was 5×10^4 cells per ml.

For microscopic experiments cells were incubated with 1–8 μM of conjugate **BChl-NI** for 1–3 h in a complete medium at 37 °C. Detailed intracellular distribution of conjugate was studied with the Leica SP2 confocal laser scanning microscope (Leica, Germany). Conjugate fluorescence was excited with 488 nm (fits well to the absorption band of NI chromophore) and 514 nm (fits well to the absorption band of BChl chromophore) light. An emission in the 500–600 nm spectral range corresponding to NI unit was registered with a photomultiplier. An emission in the range 730–1000 nm corresponding to PS was registered with a highly sensitive avalanche photodiode.

Intracellular formation of photoinduced reactive oxygen species (ROS) was measured using 2',7'-dichlorofluorescein diacetate (DCFDA). Cells were incubated with 1 μM **BChl-NI** for 3 h and during last 30 min with 25 μM DCFDA. Then cells were irradiated (22 ± 2 mW cm^{-2}) with a halogen lamp (500 W) through a water filter (thickness of 5 cm) and a band-pass filter (transmission 660–1000 nm) for 15 min and analyzed by confocal microscopy. Fluorescence was

View Article Online
DOI: 10.1039/C7CP04449F

excited with 488 nm and registered in the 500–540 nm (DCFDA) and 600–650 nm (NI) regions. Cells incubated with DCFDA and **BChl-NI** without irradiation as well as cells incubated with **BChl-NI** and irradiated without DCFDA were used as a control.

To clarify the cellular mechanisms of **BChl-NI** transport, cells were thoroughly washed with a warm medium (37 °C) without serum, pre-incubated with chlorpromazine (30 μM for 30 min), or methyl-β-cyclodextrin (4 mM for 30 min) in a serum-deprived medium (37 °C) and further incubated in the presence of **BChl-NI** (4 μM for 70 min) at 37 °C. To study influence of temperature, cells were incubated with **BChl-NI** (4 μM for 70 min) at 8 °C.

In the confocal microscopy measurements, lateral and axial resolutions were ca. 0.2 and 1.5 μm respectively. Confocal microspectroscopy studies were performed at the 488 nm excitation using an experimental setup described elsewhere.[55]

For cell survival studies, conjugate **BChl-NI** was added to cells (0.04–8 μM with a two-fold increment). Control cells were incubated with equivalent concentrations of Cremophor EL. The cytotoxicity was estimated after incubation of cells with conjugate or Cremophor EL alone for 6 h in the dark. The photoinduced cytotoxicity was measured on cells incubated with conjugate or Cremophor EL alone for 3 h and irradiated as described above. After irradiation the cells were further incubated for 3 h and examined for viability. All the experiments were performed in duplicate. To evaluate cell viability, cells were stained with Hoechst 33342 (stains all cells) and propidium iodide (stains dead cells) and analyzed with a fluorescence microscope as described elsewhere.[56,57] Irradiation of control cells without **BChl-NI** did not induce any cytotoxicity at the irradiation conditions used.

View Article Online
DOI: 10.1039/C7CP04449F

3. Results and discussion

Steady-state spectroscopic properties. Absorption and emission characteristics of conjugate **BChl-NI** and monochromophoric derivatives **BChl** and **NI4** are presented in Fig.1 and Table 1. As it can be seen from Fig.1a,c, absorption spectrum of **BChl-NI** shows the presence of four bands with maxima at 354, 481, 515 and 747 nm corresponding to electronic transitions in naphthalimide (481 nm) and bacteriochlorin (354, 515 and 747 nm) moieties. Although the position and intensity of characteristic Q and Soret bands of bacteriochlorin core in the conjugate are essentially the same as those in equimolar mixture of **BChl** and **NI4** (Fig.1c), naphthalimide ICT absorption is observed at slightly higher wavelengths. This red shift could be attributed to incorporation of electron withdrawing triazole group in the *N*-butyl substituent of compound **NI4**, which enhances the ICT.

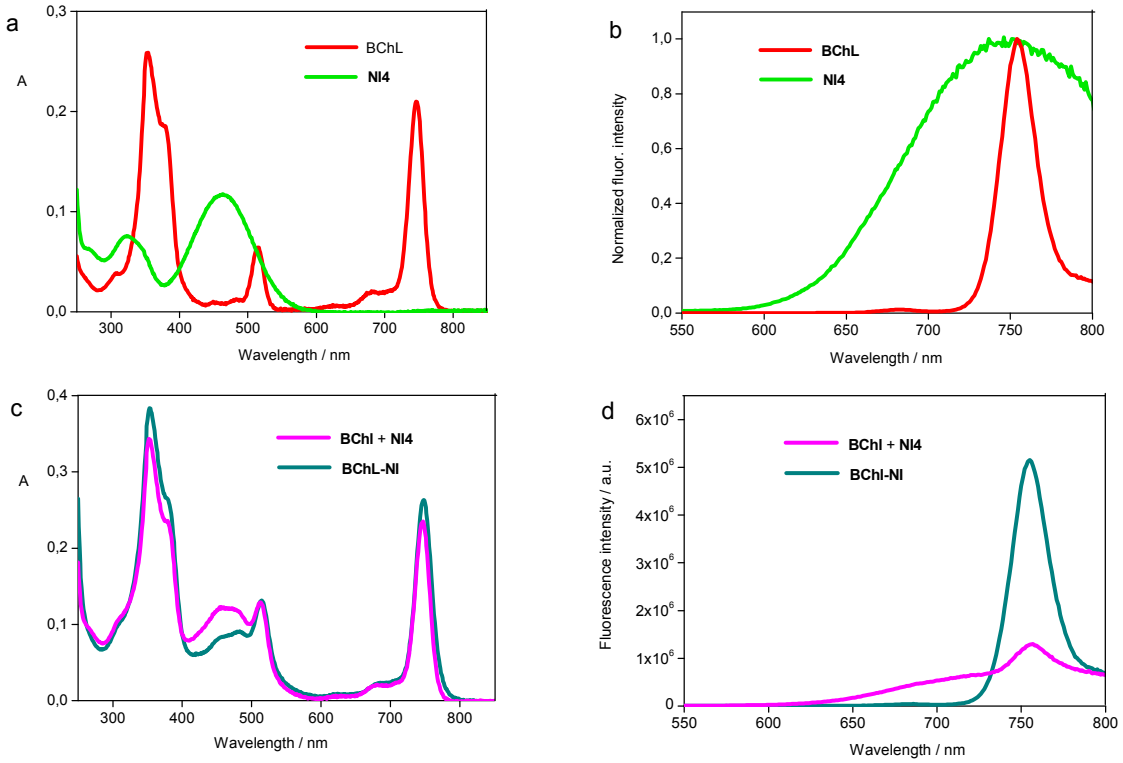

Fig.1. UV/Vis absorption (a,c) and fluorescence emission (b, d) spectra of compounds **BChl**, **NI4**, **BChl-NI** and equimolar mixture of **BChl** and **NI4** (denoted as «**BChl** + **NI4**») in acetonitrile. Excitation wavelength is 460 nm for **NI4**, **BChl-NI**, **BChl+NI4** and 515 nm for **BChl**. Concentration of all compounds – $4.7 \cdot 10^{-6}$ M.

Table 1. Photophysical characteristics of compounds **BChl**, **NI** and **BChl-NI** in acetonitrile.[a]

				Intramolecular RET in **BChl-NI**					
				Förster theory		Experiment			
	λ_{max}^{abs}/nm	$\lambda_{max}^{fl}(\lambda_{ex})$/nm	φ^{fl}	k_{RET1}/ s^{-1}	Φ_{RET1}	k_{RET1}/ s^{-1}	Φ_{RET1}	Φ_{RET2}	$\Phi_{\Delta}(\lambda_{ex}$/nm)
NI4	462	743 (460)	0.032	–	–	–	–	–	–
BChl	353; 515; 746	755 (515)	0.016	–	–	–	–	–	0.79 (510)
BChl-NI	354; 481; 515; 747	755 (460)	0.023	$0.57 \cdot 10^{12}$	0.995	$1.89 \cdot 10^{12}$	0.999	0.981	0.82 (510)

[a]Quantum yield of generation of singlet oxygen (Φ_{Δ}) is measured in acetone.

View Article Online
DOI: 10.1039/C7CP04449F

Fluorescence emission maxima of **BChl** and **NI4** appear at close λ values, however, naphthalimide spectrum is much more broad and substantially drops into IR region (Fig.1b). In the case of equimolar mixture, excitation with 460 nm light which is mostly absorbed by **NI4** results in the emission band having the same feature as that of individual naphthalimide dye but interfered to some extent by the sharp collateral peak of the **BChl** fluorescence (Fig.1d). Interestingly, the spectrum of conjugate **BChl-NI** where two photoactive units are covalently linked is found to be different (Fig.1d). Under the excitation at 460 nm, **BChl-NI** demonstrates only the characteristic band of bacteriochlorin, whereas naphthalimide fluorescence is completely quenched. This observation implies that in the conjugate, efficient energy transfer from the naphthalimide to bacteriochlorin fragment may occur. To get deeper insight into the nature of processes in the excited state of **BChl-NI** molecule we further studied transient absorption (TRABS) spectra of this system.

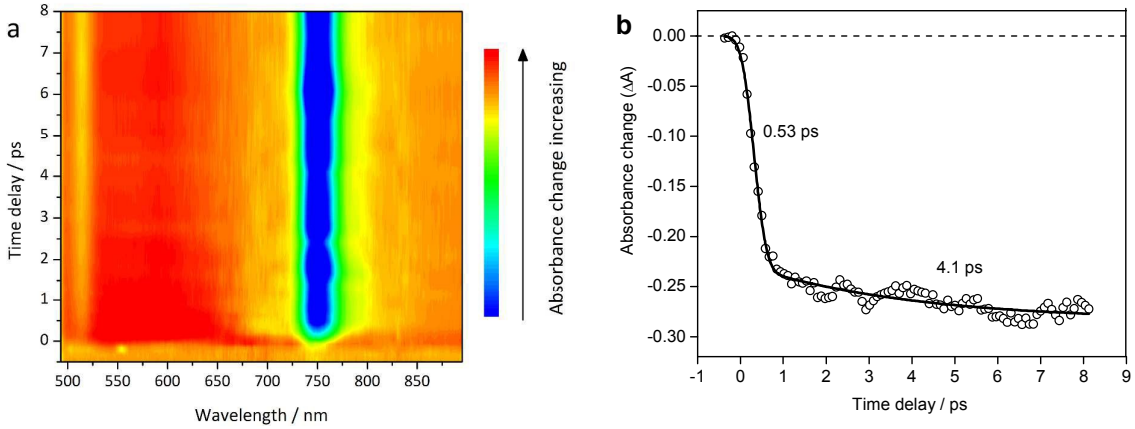

Fig.2. TRABS spectral map with subpicosecond time resolution (a) and TRABS kinetics at 750 nm (b) of **BChl-NI** in acetonitrile. Excitation wavelength – 470 nm.

Transient absorption spectroscopy. A representative result of a pump-probe experiment for **BChl-NI**, *i.e.* a map of absorbance changes after the laser pulse in delay-wavelength coordinates is displayed in Fig.2a. The excitation of naphthalimide chromophore with 470 nm light produced the negative signal at 750 nm. In accordance with the position of the long wavelength absorption band of **BChl** (Fig.1a), this signal can be ascribed to the ground state bleaching of bacteriochlorin in the conjugate.* Another feature of the TRABS map shown in Fig.1a is a broad positive band stretching from 500 to 680 nm. Probably, this spectral region covers the area where absorption signals of singlet (S_1) states of both chromophores are located.

* Apparently, the contribution of stimulated emission to the negative signal at 750 nm is relatively small, because of a high value of radiative lifetime (τ_r) of bacterioclorin. Radiative lifetime is known to be the ratio of excited singlet state lifetime to the fluorescence quantum yield. From the data presented in Fig.2 and Table 1, $\tau_r = 2\ \text{ns}/0.016 = 125\ \text{ns}$. Such high τ_r value explains low radiative rate constant ($k_r = 1/\tau_r$) and low propability of stimulated emission as a result.

View Article Online
DOI: 10.1039/C7CP04449F

One can also see that the appearance of negative band on a time scale occurs not immediately after the excitation pulse and proceeds with a characteristic time of 0.53 ps as obtained from the TRABS time profile (Fig.2b).[†] Hence, the initially formed naphthalimide excited state should participate in a kind of a fast non-radiative process more likely to be the resonance energy transfer (RET). The rate constant of RET (k_{RET1}) can be estimated from the known characteristic time as $1/0.53 \cdot 10^{-12}$ s (see Table 1 for the value of k_{RET1}). Quantum efficiency of intramolecular RET (Φ_{RET1}) is expressed as the ratio of k_{RET1} to the sum of rate constants of all other possible processes in the S_1 state of a donor:

$$\Phi_{\mathrm{RET1}} = \frac{k_{\mathrm{RET1}}}{k_{\mathrm{RET1}} + k_{\mathrm{r}} + k_{\mathrm{nr}}} = \frac{k_{\mathrm{RET1}}}{k_{\mathrm{RET1}} + {\tau_{\mathrm{D,0}}}^{-1}} \quad (3)$$

In the Eq.(3) k_{r} is the radiative rate constant of naphthalimide chromophore, and k_{nr} describes its non-radiative relaxation which is not related to energy transfer. To estimate the sum ($k_{\mathrm{r}} + k_{\mathrm{nr}}$) we used the value inversely proportional to the fluorescence lifetime of compound **NI4** ($\tau_{\mathrm{D,0}} = 0.38$ ns),[44] where RET process is not realized. The obtained value of Φ_{RET1} was found to be close to unity (Table 1) indicating highly efficient RET in the conjugate **BChl-NI**. Additionally, calculations of k_{RET1} and Φ_{RET1} by the Förster model[58] testify to the same result. The details of these calculations are shown in Supplementary Information.

Further evolution of TRABS signals of bacteriochlorin unit in **BChl-NI** can be followed by using the spectral map with nanosecond resolution (Fig.3a). The horizontal cuts of this map at a given time delay give us the TRABS spectra at these delays. The spectrum immediately after excitation is shown blue in Fig. 3b. In this spectrum, we can see broad absorption band of bacteriochlorin singlet state (several $S_1 \rightarrow S_n$ transitions could contribute) in the range of 400-650 nm formed as a result of energy transfer[‡] and negative features at 515 and 700 nm corresponding to the ground state bleaching. Kinetics of absorption at 600 nm (Fig.3c) clearly shows that S_1 state relaxes within 2 ns at which it converts to some long-lived species presumably regarded as triplets. Thus, spectrum after 40 ns (Fig.3b, red line) shows us absorption of T_1 state.

The lifetime of bacteriochlorin triplet state was found to be dramatically affected by the presence of oxygen. Whereas the degased solution exhibited single exponential decay with the time constant of 19 μs (τ_{T}), in the case of air saturated sample, the observed lifetime was 0.355 μs ($\tau_{\mathrm{T}}^{\mathrm{O_2}}$) (Fig.3c,d). Considering the difference in τ_{T} and $\tau_{\mathrm{T}}^{\mathrm{O_2}}$ values, one can conclude that the

[†] Characteristic time $\tau_2 = 4.1$ ps shown in Fig.2b describes the relaxation of the singlet excited state of bacteriochlorin. Probably, positive signal of $S_1 \rightarrow S_n$ absorption has non-zero intensity at around 750 nm which tends to decrease upon increasing of time delay. Thus, negative signal at 750 nm is becoming more and more negative even after fast process with $\tau_1 = 0.53$ ps is completed.

[‡] Energy transfer process is not visible in this map; it can be perceived with the aid of the subpicosecond experiment described above.

View Article Online
DOI: 10.1039/C7CP04449F

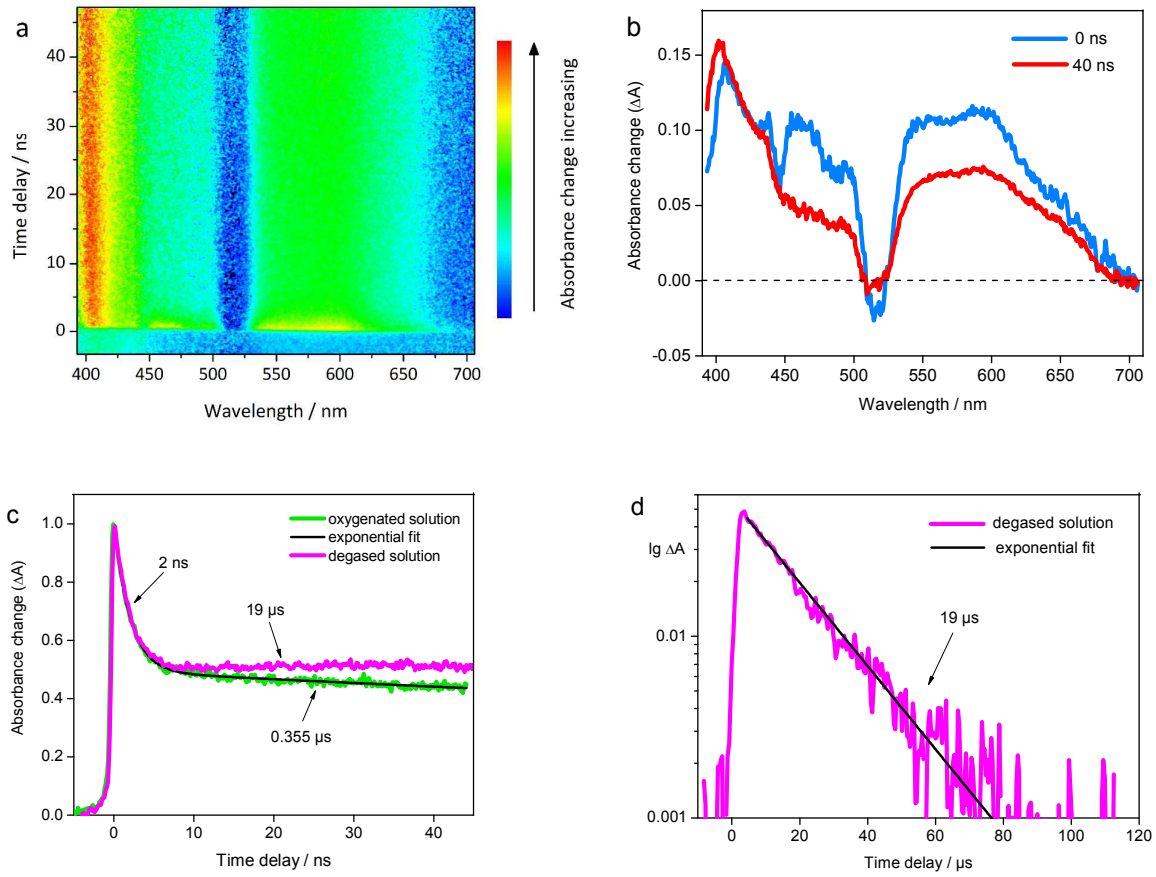

Fig.3. TRABS spectral map (a) with nanosecond time resolution, TRABS spectra at different time delays (b) and TRABS kinetic curves at 600 nm in the presence and absence of oxygen (c, d) of **BChl-NI** in acetonitrile. Excitation wavelength – 440 nm. Spectral map has negative perturbed signal at 440 nm induced by the filter rejecting this wavelength.

excitation energy is transferred from PS unit to molecular oxygen upon collisions which leads to formation of $^1O_2$ and PS in the ground state. The efficiency of this process given as Φ_{RET2} was calculated by the Eq.(4).

$$\Phi_{RET2} = 1 - \frac{\tau_T^{O_2}}{\tau_T} \quad (4)$$

As evident from the obtained value of Φ_{RET2} (0.981, see Table 1), bacteriochlorin in **BChl-NI** works as an excellent photosensitizer allowing generation of $^1O_2$ with a high quantum yield.

Photosensitizing activity. Singlet oxygen ($^1O_2$) is thought to be a key cytotoxic agent in the photodynamic inactivation of living cells.[59,60] It is formed as a result of energy transfer from photosensitizer triplet state to molecular oxygen. Photosensitized $^1O_2$ formation was studied using 1,3-diphenylisobenzofuran (DPBF) as a singlet oxygen trap. Interaction of DPBF with $^1O_2$ is known to be purely chemical, resulting in formation of colorless endoperoxides.[53,54] This process causes bleaching of the main maximum of DPBF at 414 nm. Fig. 4 illustrates one of the

View Article Online
DOI: 10.1039/C7CP04449F

experiments on photosensitized bleaching of DPBF in a solution of the conjugate **BChl-NI** in acetone under illumination with green (510 nm) light which is absorbed by both chromophores. Rapid photobleaching of DPBF was also detected in solution of free bacteriochlorin **BChl** (Fig.S24, Supplementary Information). This observation is consistent with the results of previous studies which showed that metal-free bacteriochlorins efficiently photosensitized singlet oxygen formation in air saturated solutions.[61,62] In solution of the free naphthalimide dye, photobleaching of the trap was not found (Fig.S25, Supplementaty Information). Quantum yields of singlet oxygen production of **BChl** and **BChl-NI** under the excitation at 510 nm were found to be 0.79 and 0.82 respectively (Table 1). Such close values indicate that photosensitizing activity of the naphthalimide dye in the conjugate is, apparently, caused by efficient energy transfer from the dye to the bacteriochlorin, which is in a good agreement with the above time-resolved studies of **BChl-NI**, and the presence of naphthalimide fragment in **BChl-NI** does not decrease the ability of PS core to generate $^1O_2$.

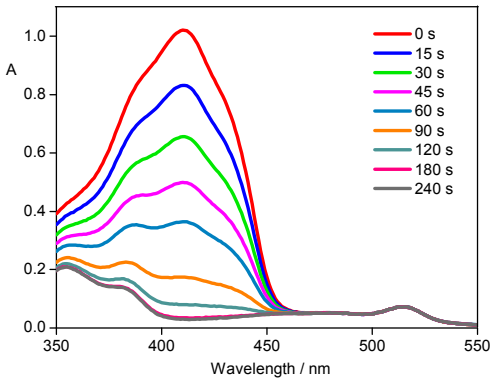

Fig.4. Changes in the UV/Vis absorption spectrum of a mixed solution containing the conjugate **BChl-NI** ($2.6\cdot10^{-6}$ M) and DPBF ($4.0\cdot10^{-5}$ M) in acetone upon irradiation at 510 nm.

***In vitro* studies of conjugate BChl-NI**. As confirmed with confocal microspectroscopy and confocal laser scanning microscopy, conjugate penetrates into cancer A549 cells (Fig.5,6). Intracellular fluorescence spectra of **BChl-NI** were measured by confocal microspectrosopy with the 488 nm excitation wavelength, which fitted well to the absorption band of the NI moiety of the conjugate. Typical intracellular emission spectrum of **BChl-NI** is shown in Fig.5e. Its shape and long-wavelength maximum (757 nm) correspond to the fluorescence of bacteriochlorin moiety. Intense illumination of a cell with the 488 nm light leads to the changes in intracellular fluorescence spectra of **BChl-NI**: a band with the 757 nm maximum disappears due to photobleaching of acceptor (BChl), and a donor (NI) fluorescence is restored, which has a maximum at ca. 600 nm (Fig.5f). These changes confirm RET between NI and BChl chromophores in cells and show that polarity of cellular microenviroment is similar to the

View Article Online
DOI: 10.1039/C7CP04449F

polarity of diethyl ether solution (ε = 4.3), where NI chromophore has fluorescence maximum at 608 nm.[44] §

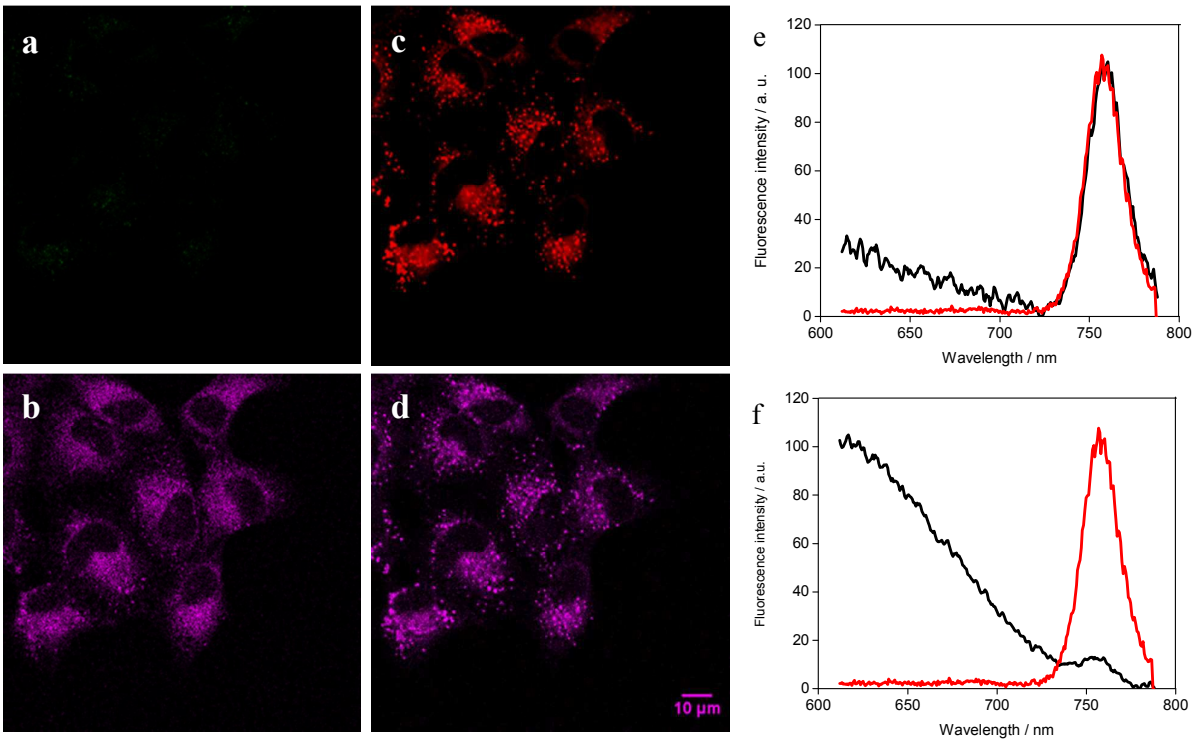

Fig.5. Intracellular distribution of **BChl-NI** fluorescence in A549 cells. Distribution of fluorescence in the 550-650 nm (a, c) and >730 nm (b, d) ranges at the low power 488 nm excitation before (a,b) and after (c,d) the high power prolonged illumination (photobleaching) of cells with the 488 nm wavelength. (e,f) Examples of intracellular fluorescence spectra of **BChl-NI** (black line) at the 488 nm excitation before (e) and after (f) the high power prolonged illumination (photobleaching) of cells. Red line – fluorescence spectrum of **Bchl** in 1% Chremophor EL solution. Spectra are normalized to the highest intensity. Cells were incubated with 2 µM of **BChl-NI** for 3 h.

In agreement with microspectroscopy studies, confocal laser scanning microscopy reveals intracellular fluorescence of **BChl-NI** in the range of 730 nm and longer wavelengths (at the excitation of 488 or 514 nm) and absence of fluorescence in the 500–650 nm range (Fig.5a,b). As clearly seen (Fig.5b, Fig.6), conjugate accumulates in cytoplasm of A549 cells and does not penetrate into the nucleus. In cytoplasm, **Bchl-NI** has diffuse distribution. The pattern of intracellular distribution is similar at different extracellular concentrations of **BChl-NI** and different incubation times of cells with the conjugate (Fig.6). An increase in extracellular concentration of the conjugate from 2 to 8 µM and incubation time from 1 to 3 h increases moderately intracellular fluorescence that indicates to saturation of intracellular accumulation of **BChl-NI** at concentrations higher than 4 µM and incubation time of 3 h.

§ Similar blue shift of naphthalimide emission band was also observed in rabbit blood serum. However, RET between NI and BChl chromophores remains highly efficient as it is in CH_3CN (the solvent we used for the photophysical studies, ε = 37.5). This was demonstrated by the comparison of emission spectra of conjugate **BChl-NI** in rabbit blood serum with the corresponding spectra of equimolar mixture containing individual photosensitizer **BChl** and naphthalimide dye (see Supplementary information, Fig.S26).

View Article Online
DOI: 10.1039/C7CP04449F

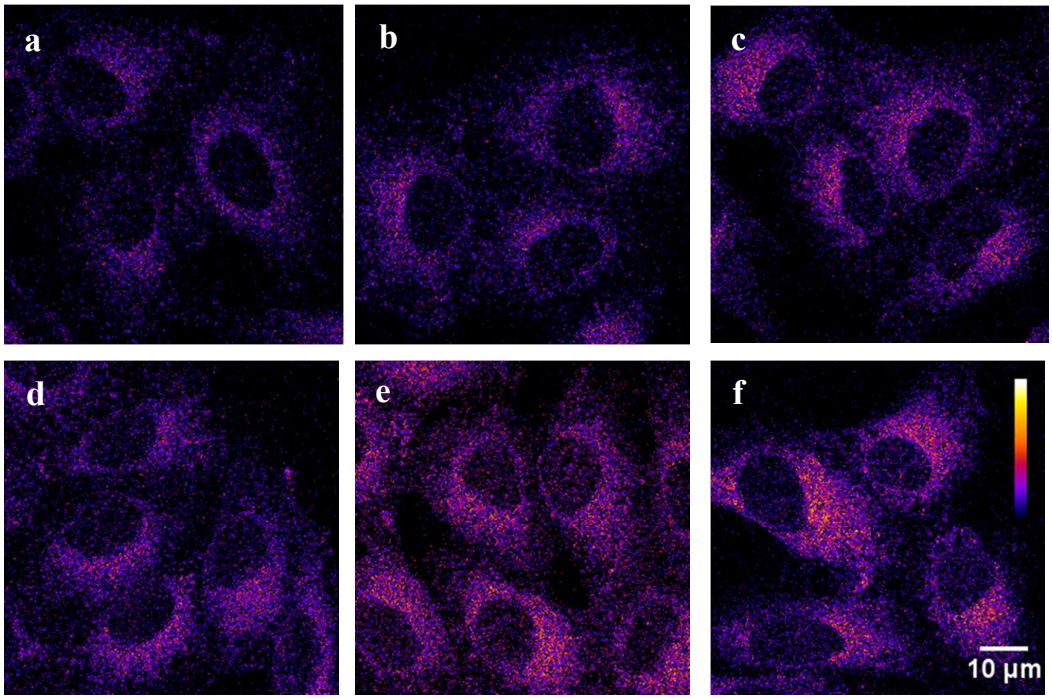

Fig.6. Intracellular accumulation of **BChl-NI** in A549 cells. Confocal fluorescent images describing the intracellular distribution of the conjugate based on the bacteriochlorin fluorescence (exitation 514 nm, emission >730 nm). Cells were incubated with 2 (a,d), 4 (b,e) ,8 (c,f) μM conjugate for 1 h (a–c) or 3 h (d–f).

Intense prolonged illumination of cells with 488-nm or 514 nm light leads to the appearance of fluorescence in the 500-650 nm range due to photobleaching of BChl chromophore. In the course of photobleaching, the distribution of intracellular fluorescence becomes granular (Fig.5c,d) as a result of photodynamic (phototoxic) processes induced in cells.

To study the mechanism of **BChl-NI** penetration into cells, the known inhibitors of clathrin-dependent (chlorpromazine) and caveolae-dependent (methyl-*β*-cyclodextrin) endocytosis[63] were used. It was found that intracellular penetration of **BChl-NI** was not inhibited, when cells were pre-treated with chlorpromazine (inhibitor, which induces dissociation of clathrin from a cell surface) (Fig.7b) or with methyl-β-cyclodextrin (compound that depletes plasma membrane cholesterol) (Fig. 7c). Therefore, clathrin-dependent or caveolae dependent endocytosis pathways are not noticeably involved in **BChl-NI** uptake into A549 cells. A decrease in incubation temperature from 37 to 8 °C led to a threefold decrease in **BChl-NI** intracellular accumulation (Fig.7d,e).This effect can be explained by a passive diffusion of **BChl-NI** through the plasma membrane, which is affected by a decrease in membrane fluidity at a low temperature.

The studies showed that conjugate **BChl-NI** was not toxic for A549 cells at tested concentrations (<8 μM, Fig.8) without light-induced activation. At the same time, the concentration-dependent killing of cells (Fig.8) was observed upon irradiation with the red light.

View Article Online
DOI: 10.1039/C7CP04449F

In the used conditions, the photodynamic effect was achieved through the excitation of bacteriochlorin moiety. Conjugate concentrations that provides 90% and 50% photoinduced cell death are 0.70 ± 0.05 and 0.33 ± 0.05 μM respectively. These data indicate that the conjugate is an active photosensitizer, and its further investigation for anticancer photodyanmic therapy is warranted.

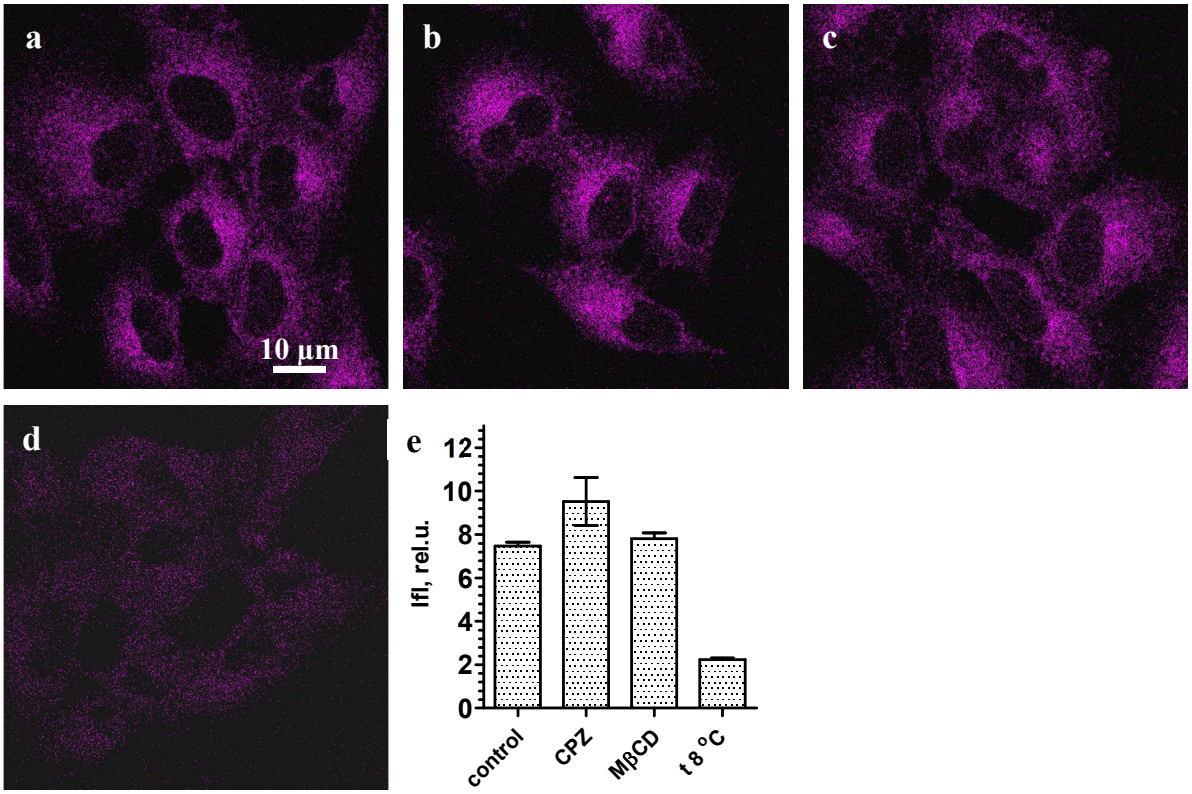

Fig.7 Study of mechanisms of intracellular penetration of **BChl-NI**. (a-d) Confocal fluorescent images showing the intracellular distribution of **BChl-NI** in control cells (a), cells pre-incubated with 30 μM chlorpromazine (b) or 4 mM methyl-β-cyclodextrin for 30 min (c) or in the cells at 8°C (d). (e) Comparison of average intracellular fluorescence intensities of **BChl-NI** at incubation regimes depicted in (a-d): CPZ, MβCD –treatment with chlorpromazine or methyl-*β*-cyclodextrin, respectively. Cells were incubated with 4 μM **BChl-NI** for 70 min at 37 °C (a-c) or 8°C (d).

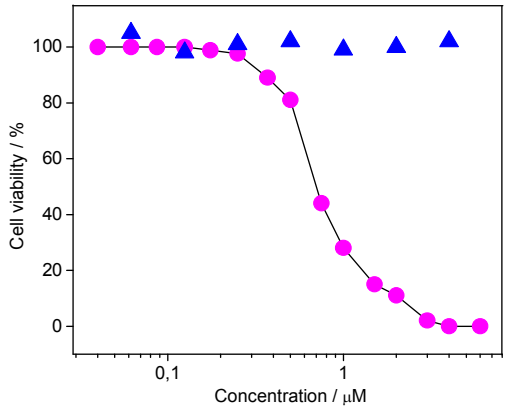

Fig.8. Concentration dependent survival of A549 cells after photodynamic treatment with the conjugate (circles). An abscissa is the photosensitizer concentration in the medium. Cells were incubated with the conjugate for 3 h, irradiated with light, and their survival was determined 3 h after irradiation. Control cells (triangles) were incubated with conjugate for 6 h without irradiation.

View Article Online
DOI: 10.1039/C7CP04449F

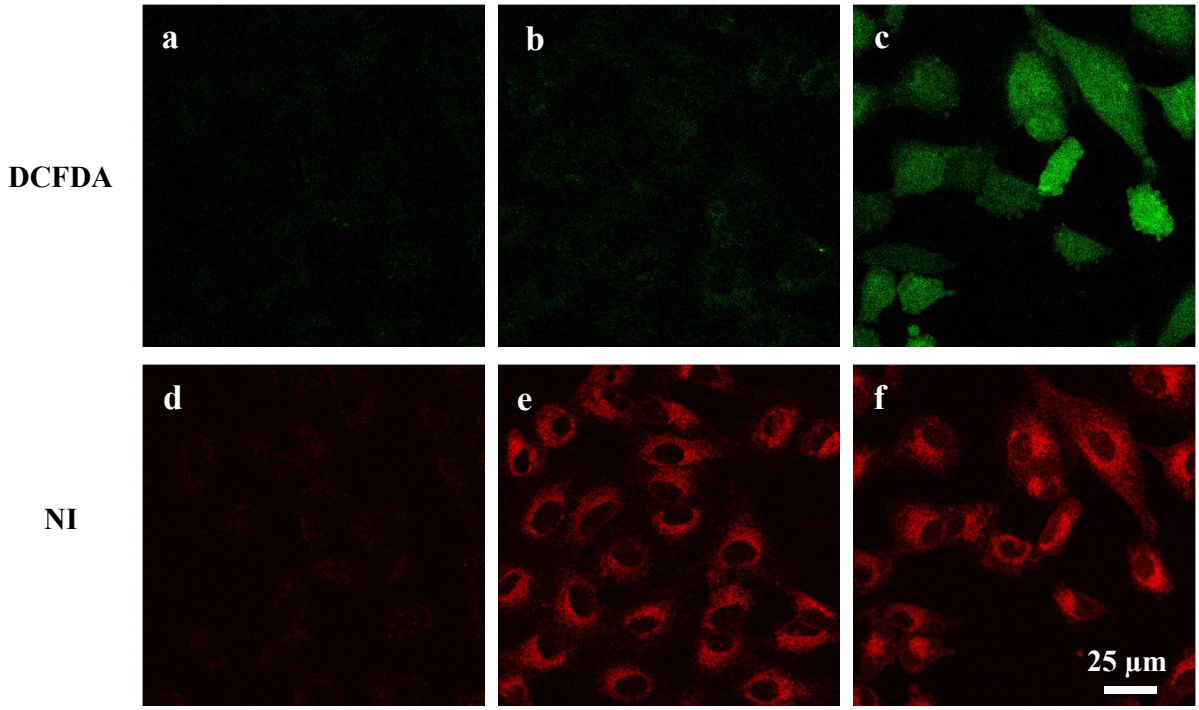

Fig.9. Verification of light-induced ROS formation in cells using DCFDA. Confocal fluorescence images show distribution of DCFDA (a-c) and NI-moiety (d-f) fluorescence in the irradiated A549 cells. Fluorescence was excited at 488 nm and registered in the 500-540 nm (DCFDA, green) and 600-650 nm (**NI**, red). (a,d) – Cells were incubated with DCFDA but without **BChl-NI** and irradiated with red light. (b,e) –Cells were incubated with **BChl-NI** but without DCFDA and irradiated. (c,f) – Cells were incubated with **BChl-NI** and DCFDA and irradiated.

To confirm the formation of reactive oxygen species (ROS) in cells under irradiation, cells were incubated with both DCFDA and **BChl-NI** and irradiated with the red light (Fig.9). In viable cells, DCFDA undergoes deacetylation to non-fluorescent 2',7'- dichlorofluorescein. This compound reacts quantitatively with ROS in cells and produces the fluorescent dye 2',7'-dichlorofluorescein. DCFDA is known to be very reactive with peroxides but can be also oxidized by other ROS.[64] Bright fluorescence of DCFDA and NI-moiety was observed in cytoplasm after irradiation (Fig.9c,f). Appearance of DCFDA fluorescence indicates ROS generation during irradiation of cells. No fluorescence of DCFDA and NI was detected in control cells without irradiation (data not shown). No fluorescence of DCFDA was observed in cells incubated with DCFDA but without **BChl-NI** and irradiated (Fig.9a) thus confirming again that **BChl-NI** does produce ROS during irradiation with the red light.

View Article Online
DOI: 10.1039/C7CP04449F

4. Conclusions

In summary, we have prepared novel bacteriochlorin–naphthalimide conjugate **BChl-NI**. Steady-state and time-resolved spectroscopical study of **BChl-NI** in solution has shown that the presence of NI fragment does not decrease the photosensitizing activity of BChl, however the fluorescence of naphthalimide is quenched due to efficient resonance energy transfer. *In vitro* results revealed high photoinduced cytotoxicity and fluorescent imaging capability that can be realized using both chromophores. Far-red absorption and fluorescence of BChl moiety makes this conjugate suitable for photodynamic treatment of deeply located tumors as well as for fluorescent imaging and navigation *in vivo*. At the same time far-red fluorescence of the conjugate is poorly detectable in cellular studies, since conventional confocal microscopes equipped with photomultiplier-based detection systems have low sensitivity in the 700–900 nm spectral range. Accordingly, photoinduced magenta-to-red[**] conversion of fluorescence can facilitate visualization of the conjugate in cellular studies. Moreover, this color conversion of **BChl-NI** fluorescence could be a useful indicator of integrity of photosensitizer moiety during irradiation of cancer cells and can help to optimize a power and dose of light during photodynamic treatment. Thus, newly synthesized conjugate **BChl-NI** is a good candidate for the next-generation "bifunctional" photosensitizer allowing PDT and fluorescent diagnostics to be performed.

Acknowledgements

O.A.F. thanks RSF project № 16-13-10226 (synthesis of naphthalimide derivatives, steady-state absorption and fluorescence spectroscopy), M.A.G. thanks RSF project № 16-13-10092 (synthesis of bacteriochlorin derivatives), G.J. thanks the Région Nouvelle-Aquitaine for financial support (time-resolved optical measurements).

[**] We used confocal laser scanning microscopy to visualize the intracellular distribution of the conjugate **BChl-NI**. Fluorescence was registered with a highly sensitive avalanche photodiode or with a photomultiplier. Both detectors record intensity of emitted light in each point of scanned specimen and do not recognize color (wavelength) of detected photons. Color of image is selected by a scientist using palettes, which are available in software. In order to provide better color reproduction, we chose a red color for NI emission in Fig.5c. Fluorescence of BChl moiety has wavelengths that are not visible to a human eye. We decided to use dark magenta color for this fluorescence in the presented images.

View Article Online
DOI: 10.1039/C7CP04449F

References

1 J. P. Celli, B. Q. Spring, I. Rizvi, C. L. Evans, K. S. Samkoe, S. Verma, B. W. Pogue, T. Hasan*, Chem. Rev.*, 2010, **110**, 2795–2838.

2 P. Agostinis, K. Berg, K.A. Cengel, T.H. Foster, A.W. Girotti, S.O. Gollnick, S.M. Hahn, M.R. Hamblin, A. Juzeniene, D. Kessel, M. Korbelik, J. Moan, P. Mroz, D. Nowis, J. Piette, B.C. Wilson, J. Golab, *CA Cancer J. Clin.*, 2011, **61**, 250–281.

3 B. W. Henderson, T. J. Dougherty, *Photochem. Photobiol.*, 1992, **55**, 145–157.

4 B. W. Henderson, T. J. Dougherty, P. B. Malone, *Prog. Clin. Biol. Res.*, 1984, **170**, 601–612.

5 B. W. Henderson, S. O. Gollnick, in: W. M. Horspool, F. Lenci (Eds.), *CRC Handbook of Organic Photochemistry and Photobiology*, second ed., CRC Press LLC, Boca Raton, 2004.

6 I. J. MacDonald, T .J. Dougherty, *J. Porphyr. Phthalocyanines*, 2001, **5**, 105–129.

7 B. C. Wilson, W. P. Jeeves, D. M. Lowe, *Photochem. Photobiol.*, 1985, **42**, 153–162.

8 D. Kessel, *Photochem. Photobiol.*, 1989, **49**, 447–452.

9 R. R. Allison, G. H. Downie, R. Cuenca, X.-H. Hu, C. J. Childs, C. H. Sibata, *Photodiagn. Photodyn. Ther.*, 2004, **1**, 27–42.

10 S. J. Bakri, P. K. Kaiser, *Expert Opin. Pharmacother.*, 2004, **5**, 195–203.

11 M. Huggett, M. Jermyn, A. Gillams, R. Illing, S. Mosse, M. Novelli, E. Kent, S. Bown, T. Hasan, B. Pogue, *Br. J. Cancer*, 2004, **110**, 1698–1704.

12 N. C. Gady, R. Granet, V. Sol, *Dyes Pigm.*, 2013, **98**, 609–614.

13 N. Patel, P. Pera, P. Joshi, M. Dukh, W. A. Tabaczynski, K. E. Siters, M. Kryman, R. R. Cheruku, F. Durrani, J. R. Missert, R. Watson, T. Y. Ohulchanskyy, E. C. Tracy, H. Baumann, R. K. Pandey, *J. Med. Chem.*, 2016, **59**, 9774–9787.

14 A. Grichine, A. Feofanov, T. Karmakova, N. Kazachkina, E. Pecherskih, R. Yakubovskaya, A. Mironov, M. Egret-Charlier, P. Vigny, *Photochem. Photobiol.*, 2001, **73**, 267–277.

15 A. Feofanov, G. Sharonov, A. Grichine, T. Karmakova, A. Pljutinskaya, V. Lebedeva, R. Ruziyev, R. Yakubovskaya, A. Mironov, M. Refregier, J.-C. Maurizot, P. Vigny, *Photochem. Photobiol.,* 2004, **79**, 172–188.

16 G. V. Sharonov, T. A. Karmakova, R. Kassies, A. D. Pljutinskaya, M. A. Grin, M. Refregiers, R. I. Yakubovskaya, A. F. Mironov, J.-C. Maurizot, P. Vigny, C. Otto, A. V. Feofanov, *Free Radic. Biol. Med.*, 2006, **40**, 407–419.

View Article Online
DOI: 10.1039/C7CP04449F

17 T. Karmakova, A. Feofanov, A. Pankratov, N. Kazachkina, A. Nazarova, R. Yakubovskaya, V. Lebedeva, R. Ruziyev, A. Mironov, J.-C. Maurizot and P. Vigny, *J. Photochem. Photobiol. B*, 2006, **82**, 28–36.

18 M. P. A. Williams, M. Ethirajan, K. Ohkubo, P. Chen, P. Pera, J. Morgan, W. H. White III, M. Shibata, S. Fukuzumi, K. M. Kadish, R. K. Pandey, *Bioconjugate Chem.*, 2011, **22**, 2283–2295.

19 N. S. James, T. Y. Ohulchanskyy, Y. Chen, P. Joshi, X. Zheng, L. N. Goswami, R. K. Pandey, *Theranostics*, 2013, **3**, 703–718.

20 N. S. James, P. Joshi, T. Y. Ohulchanskyy, Y. Chen, W. Tabaczynski, F. Durrani, M. Shibata, R. K. Pandey, *Eur. J. Med. Chem.*, 2016, **122**, 770–785.

21 P. A. Panchenko, A. N. Sergeeva, O. A. Fedorova, Yu. V. Fedorov, R. I. Reshetnikov, A. E. Schelkunova, M. A. Grin, A. F. Mironov, G. Jonusauskas, *J. Photochem. Photobiol. B*, 2014, **133**, 140–144.

22 M. A. Grin, P. V. Toukach, V. B. Tsvetkov, R. I. Reshetnikov, O. V. Kharitonova, A. S. Kozlov, A. A. Krasnovsky, A F. Mironov, *Dyes Pigm.*, 2015, **121**, 21–29.

23 N. S. James, Y. Chen, P. Joshi, T. Y. Ohulchanskyy, M. Ethirajan, M. Henary, L. Strekowsk, R. K. Pandey, *Theranostics*, 2013, **3**, 692–702.

24 H. Yanik, M. Göksel, S. Yeşilot, M. Durmuş, *Tetrahedron Lett.*, 2016, **57**, 2922–2926.

25 C. Göl, Malkoç, S. Yeşilot, M. Durmuş, *Dyes Pigm.*, 2014, **111**, 81–90.

26 V. M. Derkacheva, S. A. Mikhalenko, L. I. Solov'eva, V. I. Alekseeva, L. E. Marinina, L. P. Savina, A. V. Butenin, E. A. Luk'yanets, *Russ. J. Gen. Chem.*, 2007, **6**, 1117–1125.

27 N. Kuznetsova, D. Makarov, V. Derkacheva, L. Savvina, V. Alerseeva, L. Marinina, L. Slivka, O. Kaliya, E. Lukyanets, *J. Photochem. Photobiol. A*, 2008, **200**, 161–168.

28 L. G. F. Patrick, A. Whiting, *Dyes Pigm.*, 2002, **52**, 137–143.

29 I. Grabchev, R. Betcheva, *J. Photochem. Photobiol. A*, 2001, **142**, 73–78.

30 L. G. F. Patrick, A. Whiting, *Dyes Pigm.*, 2002, **55**, 123–132.

31 E. Martin, R. Weigand, A. Pardo, *J. Luminesc.*, 1996, **68**, 157–164.

32 W. Zhu, M. Hu, R. Yao, H. Tian, *J. Photochem. Photobiol. A*, 2003, **154**, 169–177.

33 G. Tu, Q. Zhou, Y. Cheng, Y. Geng, L. Wang, D. Ma, X. Jing, F. Wang, *Synth. Met.*, 2005, **152**, 233–236.

34 C. Coya, R. Blanco, R. Juárez, R. Gómez, R. Martínez, A. de Andrés, Á. L. Álvarez, C. Zaldo, M. M. Ramos, A. de la Peña, C. Seoane, J. L. Segura, *Eur. Polym. J.*, 2010, **46**, 1778–1789.

35 L. Song, E. A. Jares-Erijman, T. M. Jovin, *J. Photochem. Photobiol. A*, 2002, **150**, 177–185.

View Article Online
DOI: 10.1039/C7CP04449F

36 X. Meng, W. Zhu, Q. Zhang, Y. Feng, W. Tan, H. Tian, *J. Phys. Chem. B*, 2008, **112**, 15636–15645.

37 O. A. Fedorova, P. A. Panchenko, Y. V. Fedorov, F. G. Erko, J. Berthet, S. Delbaere, *J. Photochem. Photobiol. A*, 2015, **303–304**, 28–35.

38 P. A. Panchenko, O. A. Fedorova, Y. V. Fedorov, *Russ. Chem. Rev.*, 2014, **83**, 155–182.

39 R. M. Duke, E. B. Veale, F. M. Pfeffer, P. E. Kruger, T. Gunnlaugsson, *Chem. Soc. Rev.*, 2010, **39**, 3936–3953.

40 Z. Xu, J. Yoon, D. R. Spring, *Chem. Soc. Rev.*, 2010, **39**, 1996–2006.

41 Z. Xu, X. Qian, J. Cui, R. Zhang, *Tetrahedron*, 2006, **62**, 10117–10122.

42 K. Kawai, K. Kawabata, S. Tojo, T. Majima, *Bioorg. Med. Chem. Lett.*, 2002, **12**, 2363–2366.

43 X. Qian, Z. Li, Q. Yang, *Bioorg. Med. Chem. Lett.*, 2007, **15**, 6846–6851.

44 P. A. Panchenko, A. N. Arkhipova, O. A. Fedorova, Yu. V. Fedorov, M. A. Zakharko, D. E. Arkhipov, G. Jonusauskas, *Phys. Chem. Chem. Phys.*, 2017, **19**, 1244–1256.

45 P. A. Panchenko, A. N. Arkhipova, M. A. Zakharko, G. Jonusauskas, Yu. V. Fedorov, O. A. Fedorova, *Russ. Chem. Bull.*, 2016, **65**, 2444–2451.

46 A. N. Arkhipova, P. A. Panchenko, Yu. V. Fedorov, O. A. Fedorova, *Mendeleev Commun.*, 2017, **27**, 53–55.

47 Patent WO 00/33833.

48 Patent WO 2006/073419 A2.

49 J. Zhou, H. Liu, B. Jin, X. Liu, H. Fub, D. Shangguan, *J. Mater. Chem. C*, 2013, **1**, 4427–4436.

50 H.-H. Lin, Y.-Ch. Chan, J.-W. Chen, Ch.-Ch. Chang, *J. Mater. Chem*., 2011, **21**, 3170-3177.

51 S. Nad, M. Kumbhakar, H. Pal, *J. Phys. Chem. A*, 2003, **107**, 4808–4816.

52 C. L. Renschler, L. A. Harrah, *Anal. Chem.*, 1983, **55**, 798–800.

53 A. A. Krasnovsky Jr., A. S. Kozlov, Y. V. Roumbal, *Photochem. Photobiol. Sci.*, 2012, **11**, 988–997.

54 F. Wilkinson, W. P. Helman, A. B. Ross, *J. Phys. Chem. Ref. Data*, 1993, **22**, 113–262.

55 A. V. Feofanov, A. I. Nazarova, T. A. Karmakova, A. D. Pliutinskaia, A. I. Grishin, R. I. Yakubovskaya, V. S. Lebedeva, R. D. Ruziev, A. F. Mironov, J. C. Maurizot, P. Vigny, *Russ. J. Bioorg. Chem.*, 2004, **30**, 374–384.

56 A. V. Efremenko, A. A. Ignatova, A. A. Borsheva, M. A. Grin, V. I. Bregadze, I. B. Sivaev, A. F. Mironov, A. V. Feofanov, *Photochem. Photobiol. Sci.*, 2012, **11**, 645–652.

View Article Online
DOI: 10.1039/C7CP04449F

57 A. A. Ignatova, A. S. Maslova, M. P. Kirpichnikov, A. V. Feofanov, *Russ. J. Bioorg. Chem.*, 2009, **35**, 746–751.

58 J. R. Lakowicz, *Principles of Fluorescence Spectroscopy*, Springer, New York, USA, 2006.

59 T. J. Dougherty, C. Gomer, B. Henderson, G. Jori, D. Kessel, *J. Natl. Cancer Inst.*, 1998, **90**, 889–905.

60 A. A. Krasnovsky Jr., *Singlet oxygen and primary mechanisms of photodynamic therapy and photodynamic diseases*. *In: Photodynamic therapy at the cellular level*, Research Signpost, Trivandrum-695 023, 2007, 17–62.

61 A. A. Krasnovsky Jr., *Photochem. Photobiol.*, 1979, **29**, 29–36.

62 S. Y. Egorov, A. A. Krasnovsky Jr., *SPIE Proc.*, 1990, **1403**, 611–621.

63 A. I. Ivanov, *Methods Mol. Biol.*, 2008, **440**, 15–33.

64 C. P. LeBel, H. Ischiropoulos, S. C. Bondy, *Chem. Res. Toxicol.*, 1992, **5**, 227–231.